NINTH EUROPEAN ROTORCRAFT FORUM

Paper No. 4

WAKE CHARACTERISTICS AND AERODYNAMIC FORCES OF A HELICOPTER MODEL FUSELAGE

J. AMTSBERG, S.R. AHMED

DFVLR, GERMANY

September 13-15, 1983

STRESA, ITALY

Associazione Industrie Aerospaziali

Associazione Italiana di Aeronautica ed Astronautica

WAKE CHARACTERISTICS AND AERODYNAMIC FORCES OF A HELICOPTER MODEL FUSELAGE

J. Amtsberg, S.R. Ahmed
Deutsche Forschungs- und Versuchsanstalt für Luft- und Raumfahrt e.V. (DFVLR)
Braunschweig, Germany

Abstract

Helicopter fuselage aerodynamics has been relatively neglected in the past as compared to rotor aerodynamics. One of the reason for this is the extremely complex three dimensional flow environment in which a helicopter fuselage operates.

Therefore experimental investigations have been carried out to provide an insight into the complex flow field around a helicopter fuselage with emphasis on the wake structure. Results of these flow field measurements, forces and surface pressure distributions are presented.

Wake traverses reveal the existence of a pair of longitudinal vortices in the investigated downstream range of $0.31 \leq x_A/L \leq 0.34$. The angle of incidence of $\alpha = -5^o$ corresponds to the cruising speed. All measurements are carried out without rotor flow simulation.

1. Introduction

The fuselage of a helicopter is a bluff three dimensional body. Its shape is essentially determined by the need to accomodate the powerplant and the payload. One of the main aerodynamic requirements for modern helicopters is high cruising speed and good stability. As the parasite drag of a helicopter fuselage may account for 15% to 20% of the total drag, increased effort is needed to reduce it. For a given powerplant size the payoff is directly connected with a higher cruising speed and fuel economy.

A literature survey shows (ref.[1] to [17]) some work where fuselage aerodynamics have been investigated on the basis of overall forces measurements, surface pressure distributions and flow visualization with oil film and wool tuft techniques.

As the helicopter fuselage flow is dominated by extensive regions of separation in the aft body region and longitudinal vortices emanating from upswept rear end edges, a detailed study of the flow field, especially in the wake is needed to enhance the understanding of the drag creating mechanism and those effecting the stability. The enhanced understanding of the pysical phenomena in the wake can help improve the analytical models being used to compute the flow around helicopters.

2. Experimental arrangement and test procedure

The experiments on a helicopter model fuselage, Fig. 1, were performed in the open test section of the DFVLR low speed windtunnel in Göttingen [18]. This facility is a closed return windtunnel with 3 m x 3 m cross-section. One half of the model (scale 1:7) was instrumented with 218 pressure taps distributed over 24 body cross sections, Fig. 2. Scanivalves for pressure data acquisition were installed inside the model. For the tests, the model was mounted upside down on a sting, Fig. 3, about 2 m behind the nozzle.

A ten-hole directional probe, [19], [20], was employed for the flow field measurements, Fig. 4.

The arrangement of the four orifices on the conical tip is such as to make the pressure difference between one opposing pair sensitive primarily to flow incidence and the other to flow yaw. The instrument is used as a zero incidence reading device in the sense that incidence rotations are imposed until the pressure in the opposing pair of orifices is equilized. In this condition the tip axis is pointing nominally along the direction of local incidence. The pressure difference

of the other pair of orifices is a function of the local yaw angle, which is computed from calibration curves. The pressure in the central tip orifice and the mean of the pressures in the four orifices on the cylindrical sleeve of the probe is a function of the local total and static pressures respectively. The orifice on the rear end of the probe serves to indicate flow reversal. Thus magnitude and direction of the local velocity vector and the local pressures are determined. The relations between local and probe values and the formulae for the three components of the local velocity are given in Fig. 4.

The probe was mounted on a carriage which provides rectangular cartesian translations along the full length, width and height of the working section. All translational motions are effected by remotely controlled electric motors and measured by electronic counters. The probe was moved continously during surveys in the z_A-direction with x_A - and y_A - position kept fixed. The z_A - traverse was repeated for a new value of y_A which was increased in steps of 25 mm till a traverse plane from y_A = -350 mm to +350 mm and z_A = -300 mm to + 450 mm was scanned.

Tests were conducted at a wind speed of 60 m/s corresponding to a model reference length based Reynolds number of about 4 million. The ratio of model front to windtunnel nozzle area was about 1%. The moment refence point B (Fig. 2) has the coordinates x = 552 mm and z = 251 mm.

Measurements of pressure distributions were done in the angle of incidence range $-25^o \leq \alpha \leq +20^o$ in steps of 5^o; angle of yaw was varied for $0 \geq \beta \geq -30^o$ in steps of 5^o. Other angles investigated were $\alpha = -6^o, -7^o, -8^o, -9^o$ and $\beta = -2{,}5^o$. Pressure values incorporate errors of upto 0.5% of dynamic pressure.

Measurements of forces were carried out in the same range as the pressure measurements. For the data acquisition a strain gauge balance was used. Estimated errors in force measurements are ± 0.2 N and in moments measured ± 0.1 Nm.

Flow field measurements were done in section I: $x_A/L = 0.31$, section II: $x_A/L = -0.1$ and section III: $x_A/L = -0.31$ (see Fig. 4).

A completely computerized acquisition and data reduction system enabled a rapid flow field exploration. The continously acquired wake survey data was integrated over 0.2 s to arrive at the average value recorded.

The data of forces and pressure measurements were processed in a similar way. The integration time for the force measurement data was 0.6 s and for the surface pressure 2 s. Choice of these integration times is based on a calibration analysis of the system [20].

For flow visualization the non instrumented half of the model surface was sprayed with an emulsion of colouring petroleum and the wind turned on. Pictures of lee side were taken after the emulsion had dried. Cases investigated were at angle of incidence $\alpha = -5^o, 0, 10^o$ and angle of yaw $\beta = 0, -5^o, -15^o$. The complete results are given in ref. [21] to [23].

3. Discussion of experimental results

In what follows a representative set of results for cruise conditions at $\alpha = -5^o$ is presented. Influence of rotor is, however, ignored. An analysis of wake structure is attempted on the basis of local flow velocity vector V_{yz}, the pressure distribution and the oil flow pictures.

Effect of rear end upsweep, which is an important parameter, has not been investigated; this is a subject of a forthcoming experimental study.

3.1 Wake survey

A summary of wake survey results is given in Fig. 5. Velocity vector plots of V_{yz} in traverse planes I to III are shown for the cruise condition angle of incidence of $\alpha = -5^o$. The parameter varied is angle of yaw, β being 0, -5^o

and -15°. The view seen is from rear in the direction of flight.

It is seen that the wake is characterised by a pair of fully developed contra-rotating longitudinal vortices, which are also present for $\beta = -15^{\circ}$. The sense of rotation of the vortices is such that an upwash is created resulting in a decrease of lift.

The slight asymmetry of the results for $\beta = 0^{\circ}$ in Fig. 5 are probably due to model inaccuracy, inaccuracy of model alignment and an estimated flow angle uncertainty of ± 0.1 Degrees in the measurements.

The location of the origin of the longitudinal vortices could not be inferred from the wake survey results of plane I. The number stations scanned in this plane was limited due to the restricted manoeuvrability of the probe in the boom/fuselage junction area. Effect of yaw as visible from Fig. 5 is to deflect the vortex on right upwards and the one on left downwards.

Fig. 6 shows the spatial location of the vortex pair which is mainly determined by the fuselage rear end upsweep, the tail boom as well as the angle of yaw. The case studied is that of $\beta = -15^{\circ}$.

The vortex pair shown is also to be found in the wake of fast back automobiles [24]. The sense of rotation of the fuselage vortices is identical to that of the vortices in wake of automobiles with base slant angles bigger than 15°.

3.2 Flow visualization

Fig. 7 to 9 give an impression of the flow existent at $\alpha = -5^{\circ}$, 0 and 10° for the yaw angles of $\beta = 0, -5^{\circ}$ and -15°. The picture columns represent the local view, enlarged view of rear end and the view of the lee side.

$\alpha = -5^{\circ}$, Fig. 7:

For the symmetric flow situation ($\beta = 0$) the flow remains attached almost up to the periphery of the rear end. A clearly visible primary separation line is noticeable where the shear layer separates at the upswept rear end side edge. This shear layer rolls up and the vortex formed aligns itself with the main flow downstream. Under the influence of this vortex, an outward flow is induced in the dead water region producing a secondary vortex beneath the first vortex. The line of separation of this vortex lies laterally inwards beside the first separation line. The flow induced in the dead water region converges towards this secondary separation line.

Distortion of this vortex flow field with yaw can be observed in the figures 7, 8 and 9. The ensuing extremely complex vortex structure could not be conclusively analysed on the basis of the oil flow pictures presented.

An enlarged view of the oil flow picture for yaw angle $\beta = -5^{\circ}$ shown in Fig. 10, gives some details of the complex flow structure in the base vicinity. Weak vortices emanating at the rear end lower edge indicate a sense of rotation opposed to that of the main vortices. The existence of these vortices could not be detected in the wake survey. A probable reason is their dissipation at downstream stations where the wake survey was done.

The pressure distribution plots of Fig. 10 indicate positive pressure values on the fuselage underside up to section No. 11, so that the longitudinal vortices observed in the wake do not appear to originate here. This result supplements the earlier, based on oil flow pictures, made observation that the longitudinal vortices are created at the upswept fuselage rear end side edges.

$\alpha = 0$, Fig. 8:

For $\alpha = 0^{\circ}$, the vortex flow present at the base of the upswept slanted surface (Fig. 10) is enhanced. Effect of yaw shows qualitative similarity to that of $\alpha = -5^{\circ}$ case.

No wake survey was done for this test condition.

$\alpha = 10^{\circ}$, Fig. 9:

Increasing the angle of incidence appears to have a similar influence on the flow as if the rear end upsweep is decreased. This would mean in the present case that the effective rear end upsweep would be about 30°. As known from wake survey investigations of automobiles [24], this upsweep angle creates strong longitudinal vortices. The induction of a strong circulating fow in the dead water region of wake is noticeable, specially in the lower part of the slanted rear end.

It is interesting to note that the flow pattern on the rear end slanted surface undergoes drastic change for values of β between 0 and -5°. Beyond this yaw angle the flow pattern remains qualitatively same.

3.3 Pressure distributions

Pressure distributions over fuselage cross sections for cruise incidence angle $\alpha = -5^{\circ}$ is given in Figs. 11 and 12 for yaw angles $\beta = 0, -5^{\circ}, -15^{\circ}$ and -30°. Rear part fuselage sections are shown in Fig. 11, and front sections in Fig. 12. The measured pressure values are connected with spline curves.

The pressure distribution in section No. 8 and 13 correlate with the wake survey results of Fig. 5. Effect of yaw was to raise the lee side vortex and to lower the luff side vortex. This matches with pressure distributions of Fig. 11. The negative pressure peaks indicate however that under yaw the luff side vortex is stronger than the lee side vortex.

Fig. 12 indicates strong negative pressure peaks on the lee side of sections 18 to 22. These peaks however subside and are not noticeable in section 13 of Fig. 11. This strengthens the earlier made observation that the longitudinal vortices observed in the wake survey do not originate upstream of the rear end slant surface of the fuselage.

3.4 Force measurements

A sample result of the extensive three and six component force measurements is shown in Fig. 13, whereby the presentation is restricted to the three aerodynamic coefficients C_X, C_Z and C_M. The reference length and area are 1. Moment has been referred to Point B of Fig. 2.

Results of Fig. 13 show the anticipated trend for C_X, C_Z and C_M till the angle of incidence of about 10°. Beyond this an expected rise of C_X was not measured. A repetition of the measurements confirmed this trend. Tests to explain this behaviour are planned.

4. Conclusions

1. Wake of the model helicopter fuselage investigated is characterised by two strong longitudinal vortices.

2. Existence of these vortices is shown at distances beyond the tail rotor location.

3. As these vortices cause an upwash an effect on the total lift and tail rotor efficiency is expected.

4. Pressure distribution results exclude the possibility that these vortices are created elsewhere than at the upswept rear end side edges.

5. Effect of yaw appears to raise the lee-ward vortex and to lower the luff-ward vortex. Also the luff-ward vortex becomes stronger.

6. Even though the investigations were carried out without rotor flow simulation, the phenomena observed are expected to persist also with rotor flow.

References

[1] J.C. Biggers, J.L. McCloud III, F. Fattenahls, Wind-Tunnel Tests of Two Full-Scale Helicopter Fuselage, NASA TN D-1545, Ames Research Center Moffet Field, Calif., October 1962.

[2] G.E. Sweet, J.L. Jenkins Jr., Wind-Tunnel Investigation of the Drag and Static Stability Characteristics of four Helicopter Fuselage Models, NASA TN D-1363, 1962.

[3] J.L. Jenkins Jr., M.M. Winston, G.E. Sweet, A Wind-Tunnel Investigation of the Longitudinal Aerodynamic Characteristics of Two Full-Scale Helicopter Fuselage Models With Appendages NASA TN D-1364, 1962.

[4] R.M. White, A Low-Speed Wind-Tunnel Test of a 0.20 Scale Bell Helicopter 206 Fuselage Model Investigating General Aerodynamic Characteristics. Chance Vought Wind-Tunnel Test No. 100, 1961.

[5] J.Jr. Gillespie, et al, An Experimental And Analytical Investigation Of The Potential Flow Field, Boundary Layer, And Drag Of Various Helicopter Fuselage Configurations, AD - 777 798, Army Air Mobility Research And Development Laboratory, Fort Eustic, Virginia, Jan. 1974

[6] HELI - RUMPF BO - 105/-106, Modell 1:5, Photos Band III, Großer Windkanal des Eidg. Flugzeugwerkes Emmen (Schweiz)

[7] C.N. Keys, W.L. Ballauer, Analysis of the BO-105 drag and stability inverstigation wind-tunnel-tests, Boeing Vertol Rep. No. D212-10021-1, 1970.

[8] M. Venegoni, E. Magni, R. Baldassarrini, An Industrial Rationale For The Aerodynamic Design Of The Fuselage For A High Performances Light Helicopter, Paper presented at the third European Rotorcraft and Powered Lift Aircraft Forum. Paper No. 44, Aix-en-Provence, September 1977.

[9] D.R. Clark, F. Dvorak, B. Maskew, J.M. Summa, F. Woodward, "Helicopter flow field analysis", USARTL-TR-79-4, 1979.

[10] A.H. Logan, R. Marthe, D.R. Clark, A. Phelps, "An integrated analytical and experimental investigation of helicopter hub drag", presented at the 35th annual national forum of the American Helicopter Society, Washington, D.C., preprint no. 79-5, May 1979.

[11] A.H. Logan, R.W. Prouty, D.R. Clark, "Wind tunnel tests of large and small scale rotor hubs and pylons, volume I- data analysis and summary", USARTL-TR, to be published in 1980.

[12] D.R. Clark, F. Wilson, A Study Of The Effect Of Aft Fuselage Shape On Helicopter Drag, Paper presented at the sixth European Rotorcraft and Powered Lift Aircraft Forum. Paper No. 50, Bristol, September 1980.

[13] H. Mistry, R. Lamb, An investigation of drag associated with the upswept rear fuselage of a helicopter; University of Bristol, Aero Engineering Report No. 257, 1980.

[14] R.A. Hinchcliffe, P.G. Westland, The effect of sideslip on the vortices shed from the upswept rear fuselage of a helicopter, University of Bristol, Aero Engineering Report No. 267, 1981.

[15] J. Seddon, Aerodynamics Of The Helicopter Rear Fuselage Upsweep, Paper presented at the eighth European Rotorcraft Forum, Paper No. 2.12, Aix-en-Provence, September 1982.

[16] A. Renner, Sechskomponentenmessungen am Hubschraubermodell H3 zur Ermittlung der Richtungsstabilität mit verschiedenen Leitwerken, DFL-Bericht Nr. 0457, Braunschweig, 1968.

[17] P. Giese, Windkanalmessungen an einem Modellhubschrauber, IB 157-74 C 16, DFVLR, Braunschweig, 1974.

[18] F.W. Riegels, W. Wuest, Der 3-m-Windkanal der Aerodynamischen Versuchsanstalt Göttingen, Zeitschrift für Flugwissenschaften Nr. 9, pp. 222-228, 1961.

[19] S.R. Ahmed, W. Baumert, The Structur of wake flow behind road vehicles, Symposium on Aerodynamics of Transportation, (Editors T. Morel et al), ASME New York, pp. 93-103, 1979.

[20] S.R. Ahmed, Wake Structure of typical automobile shapes, Journal of Fluids Engineering, vol. 103, pp. 162-169, 1981.

[21] G. Polz, J. Quentin, J. Amtsberg, A. Kühn, Windkanaluntersuchungen zur optimalen Gestaltung von Transporthubschrauberzellen hinsichtlich Leistungsbedarf und Stabilitätsverhalten, MBB-UD-299/80, DFVLR IB129-81/10, DFVLR IB 16100-81C11, 1981

[22] A. Kühn, Windkanaluntersuchungen zur optimalen Gestaltung von Transporthubschrauberzellen hinsichtlich Leistungsbedarf und Stabilitätsverhalten, Band 1: Ergebnislisten der Druckverteilungsmessungen, IB 16100 - 81 C 39, Göttingen 1981

[23] A. Kühn, Windkanaluntersuchungen zur optimalen Gestaltung von Transporthubschrauberzellen hinsichtlich Leistungsbedarf und Stabilitätsverhalten, Band 2: Ergebnislisten der Kraftmessungen und Strömungsfeldmessungen, IB 16100 - 81 C 40, Göttingen, 1981

[24] S.R. Ahmed, Experimentelle und theoretische Untersuchungen zur Aerodynamik von Straßenfahrzeugen, DFVLR-Nachrichten 31, pp 4-7, November 1980

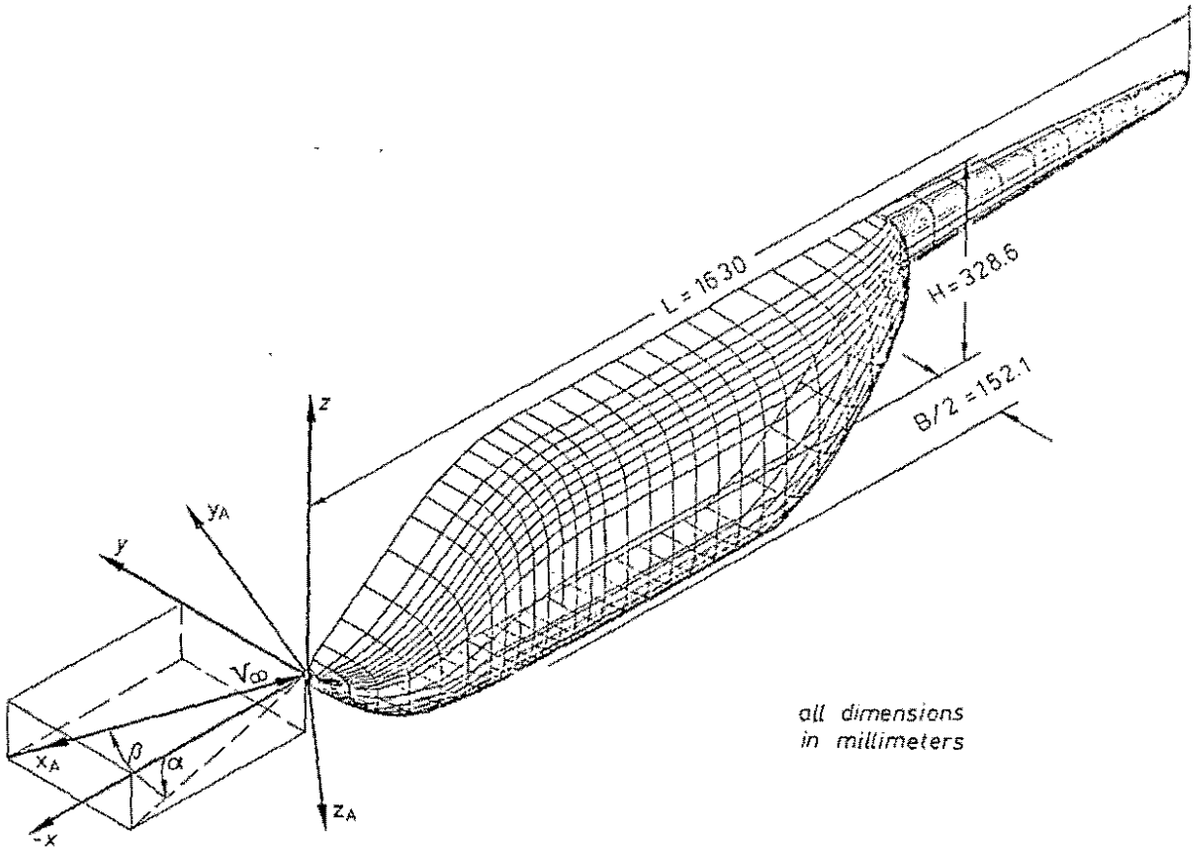

Fig. 1 Geometry of the helicopter model fuselage

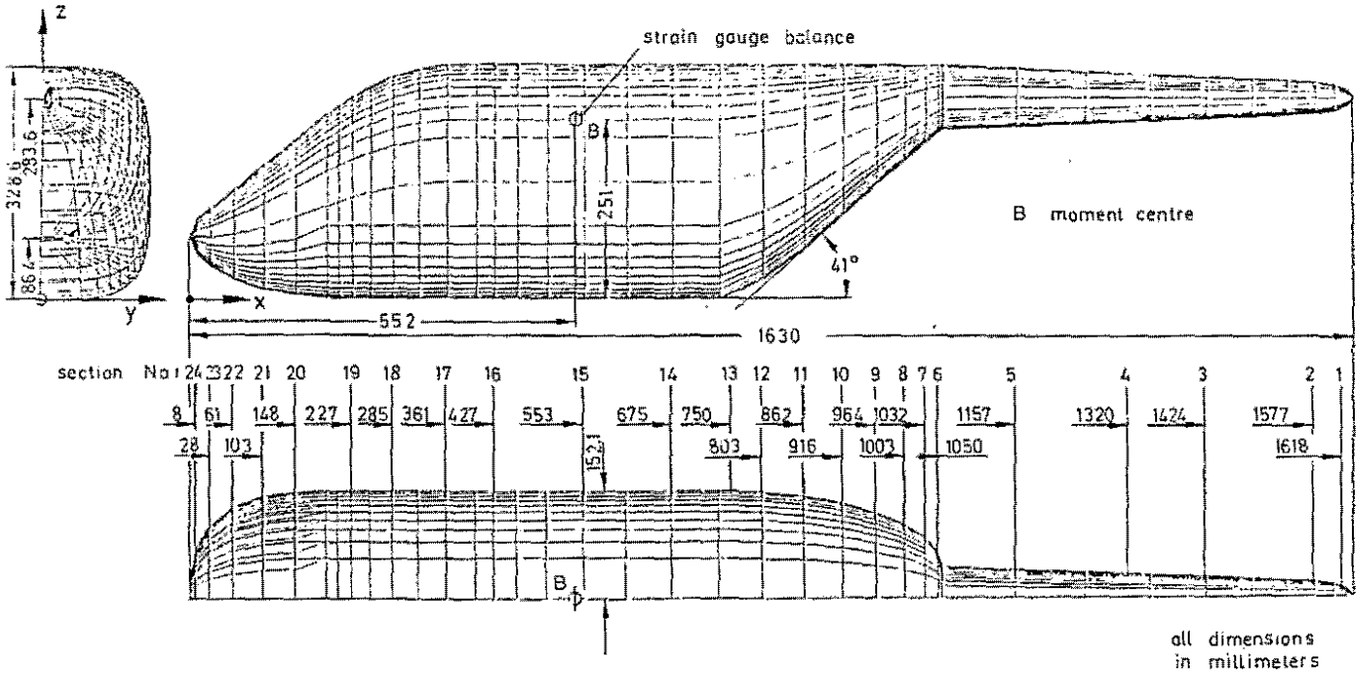

Fig. 2 Location of pressure taps and moment centre

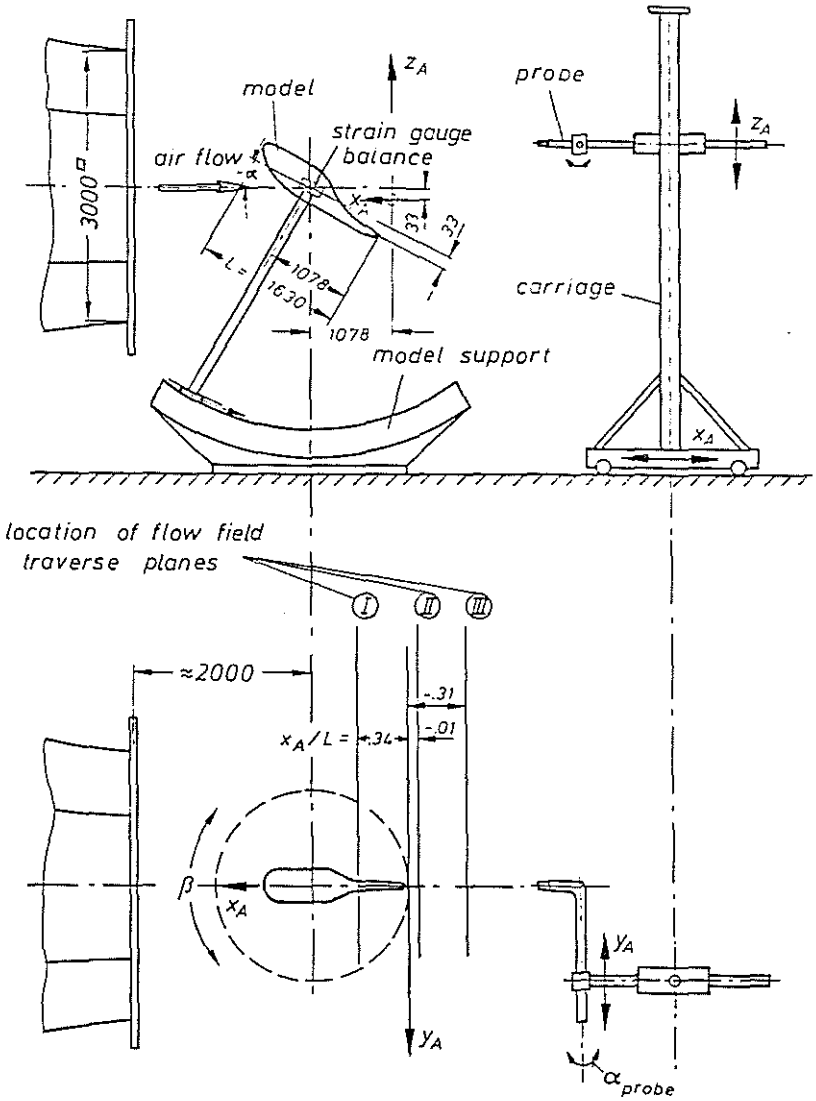

Fig. 3 Model installation in windtunnel and location of flow field traverse planes (Schematic)

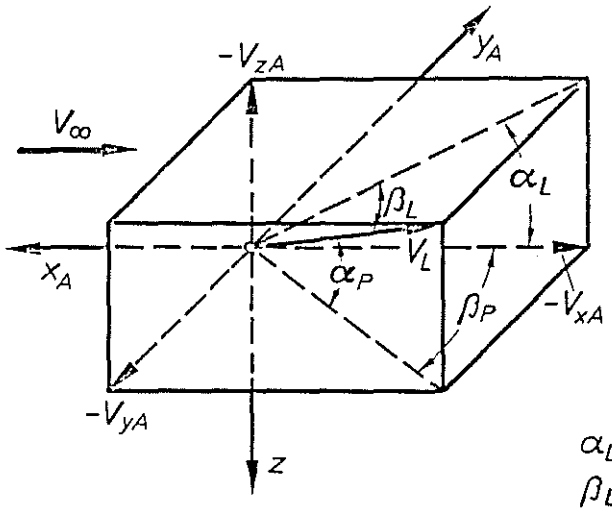

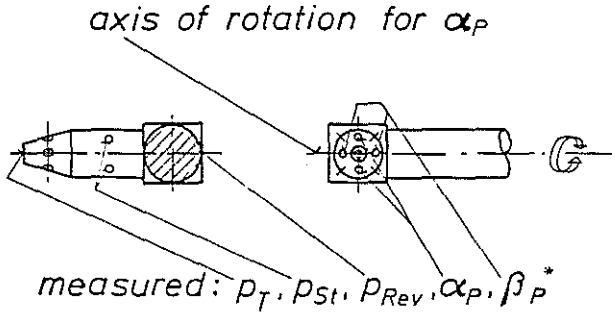

measured: p_T, p_{St}, p_{Rev}, α_P, β_P^*

$$\alpha_L = \tan^{-1}[\tan\alpha_P / \cos\beta_P]$$

$$\beta_L = \tan^{-1}[\sin\beta_P / (\cos^2\beta_P + \tan^2\alpha_P)^{1/2}]$$

$$Q_L = p_T - p_{St}, \quad V_L = (2Q_L/\rho)^{1/2}$$

$$V_{xA} = -\cos\alpha_L \cos\beta_L V_L$$

$$V_{yA} = -\sin\beta_L V_L$$

$$V_{zA} = -\sin\alpha_L \cos\beta_L V_L$$

$$V_{yz} = (V_{yA}^2 + V_{zA}^2)^{1/2}$$

Index L local values
p probe
T total
St static
Rev revers
* β_p from calibration curve

Fig. 4 Probe head details and nomenclature

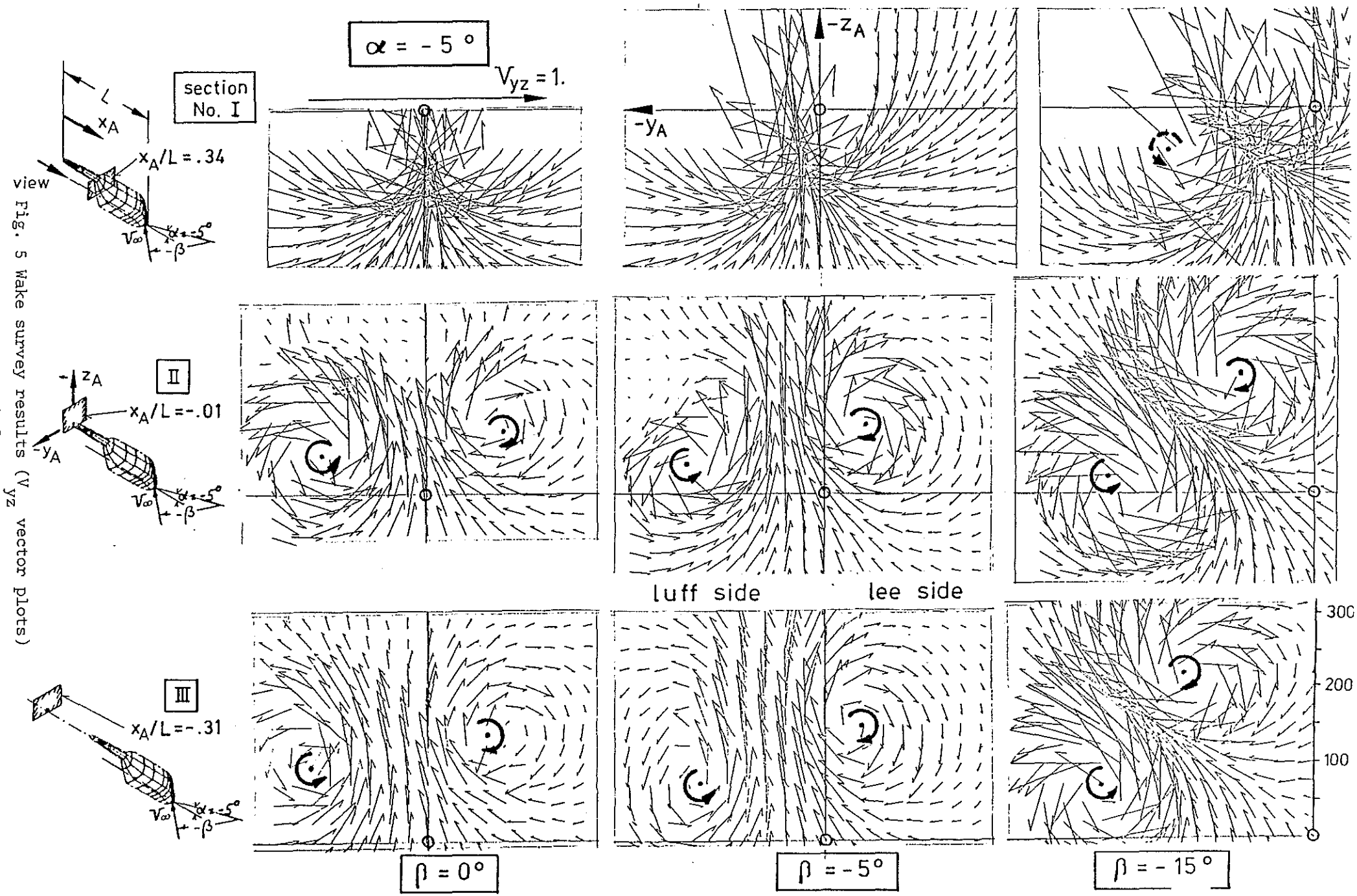

Fig. 5 Wake survey results (V_{yz} vector plots)

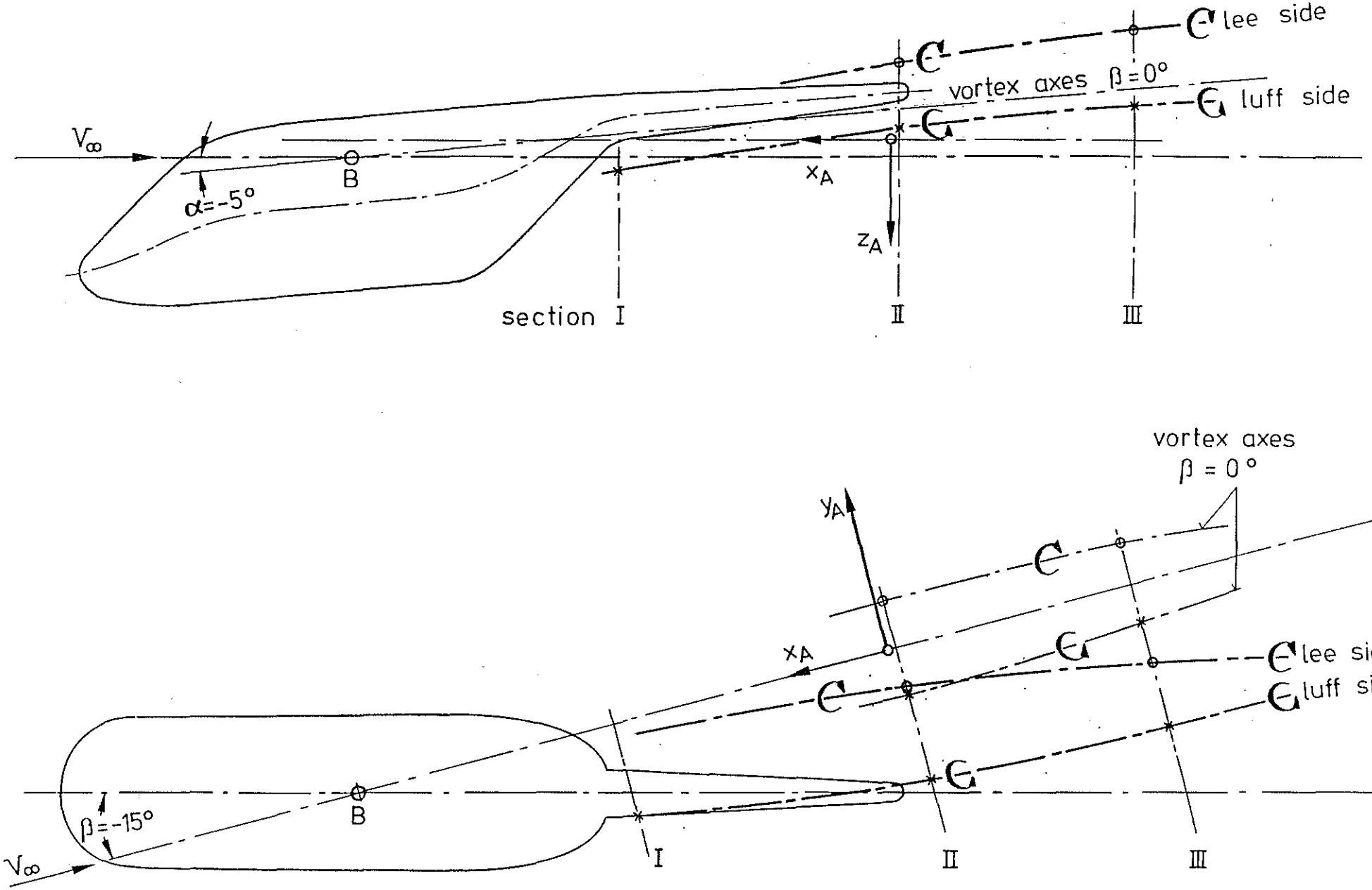

Fig. 6 Vortex core location, $\alpha = -5°$, $\beta = -15°$

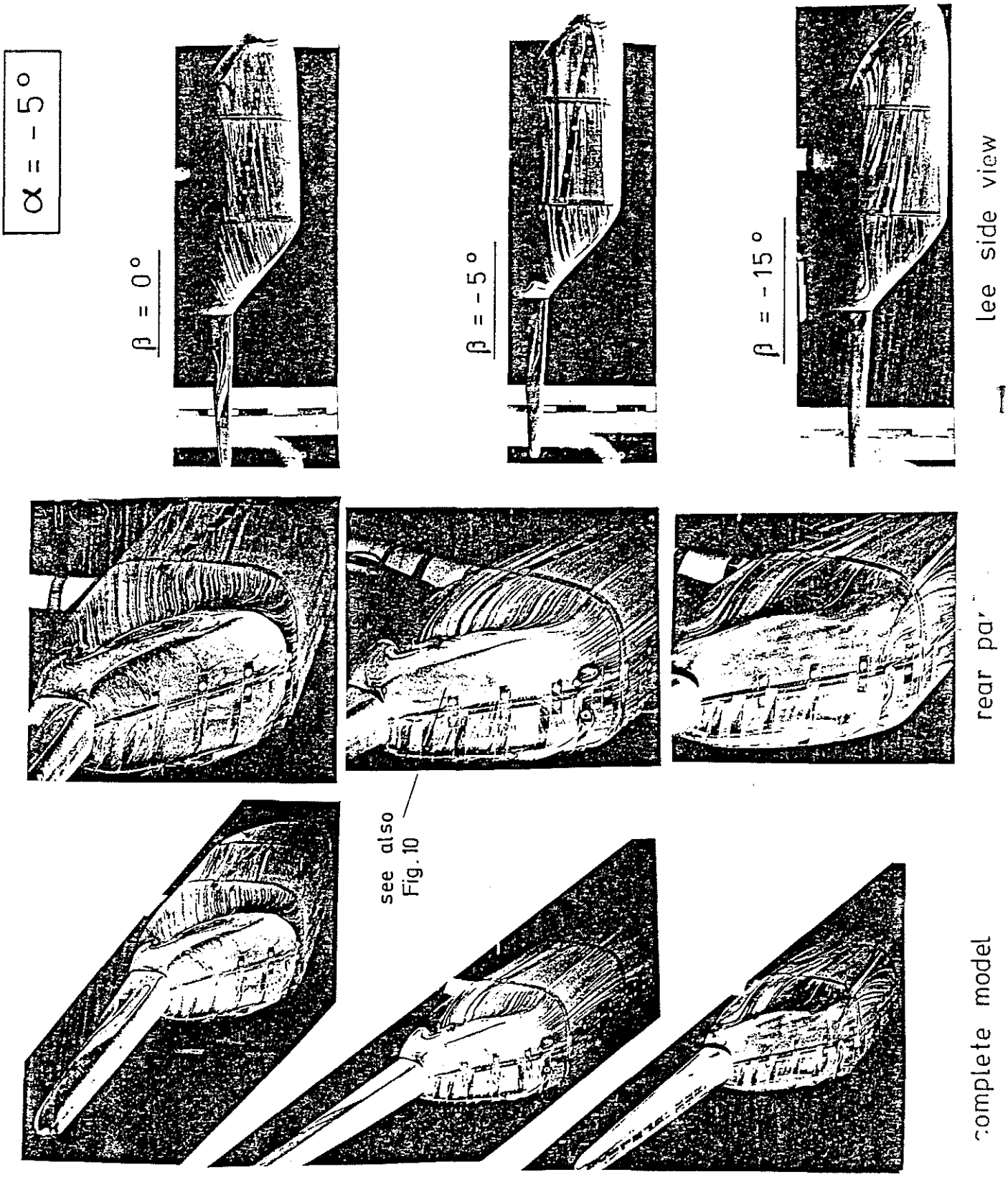

Fig. 7 Flow visualization, lee side, $\alpha = -5^{\circ}$

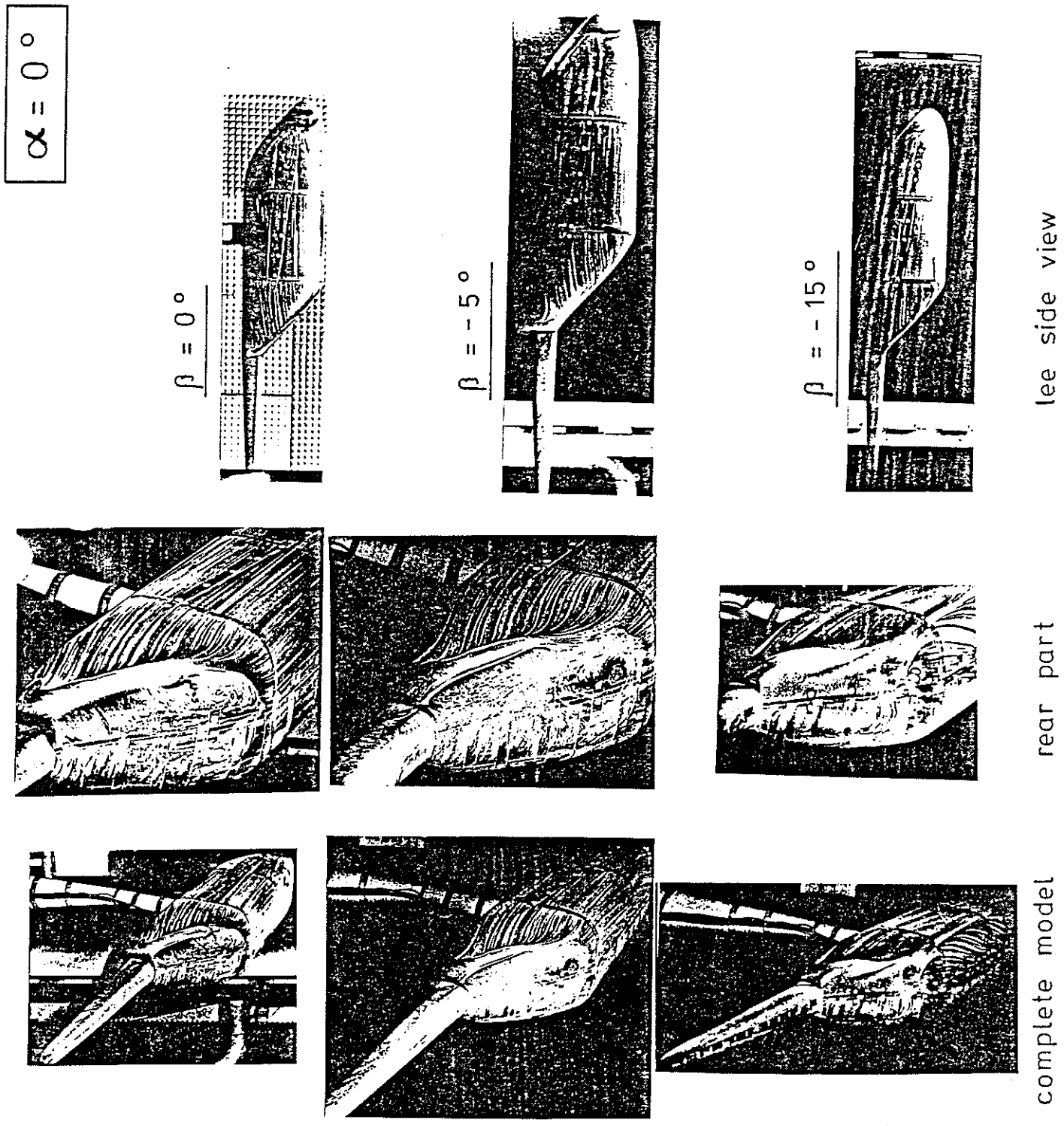

Fig. 8 Flow visualization, lee side, $\alpha = 0^{\circ}$

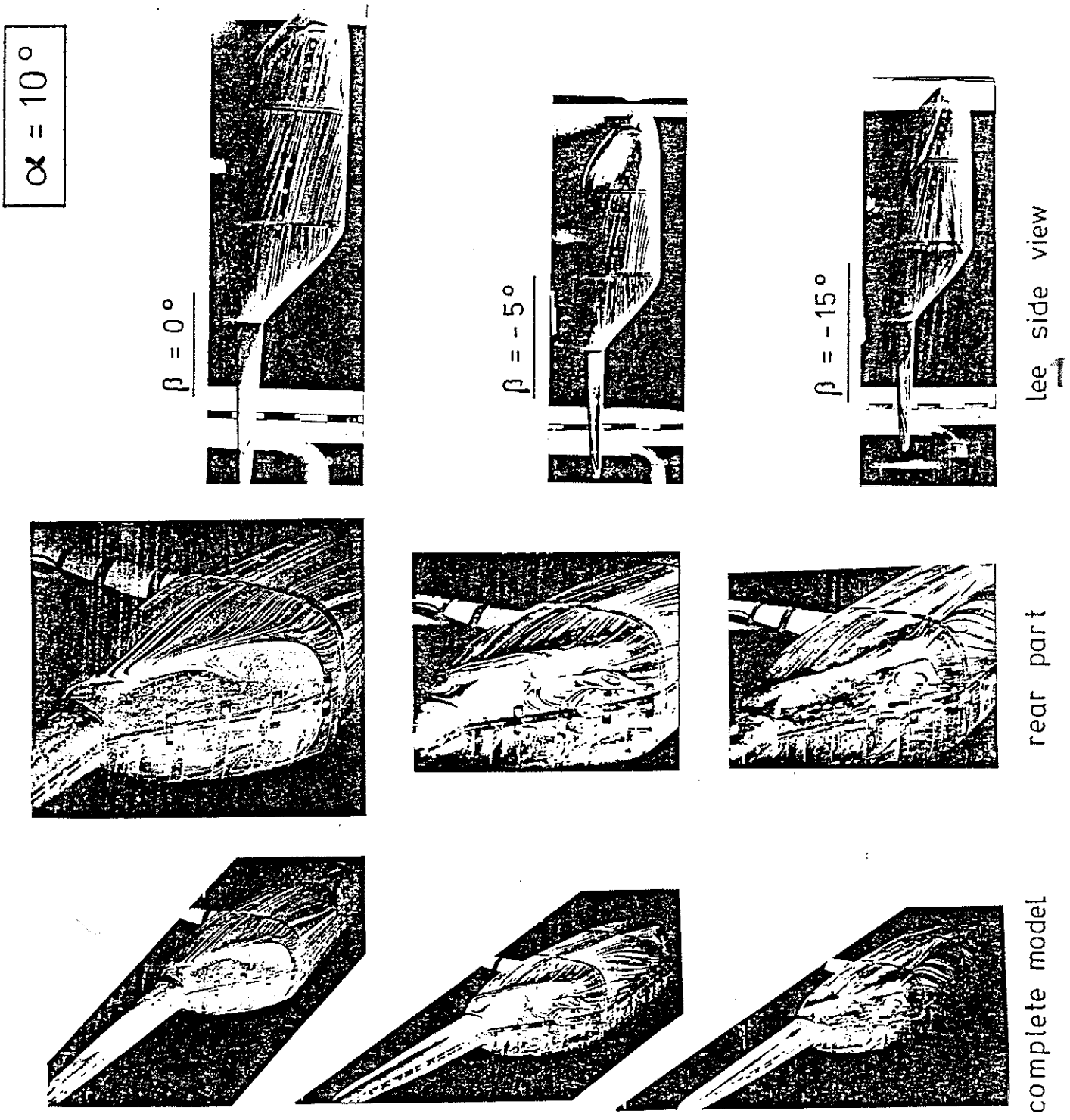

Fig. 9 Flow visualization, lee side, $\alpha = 10^{\circ}$

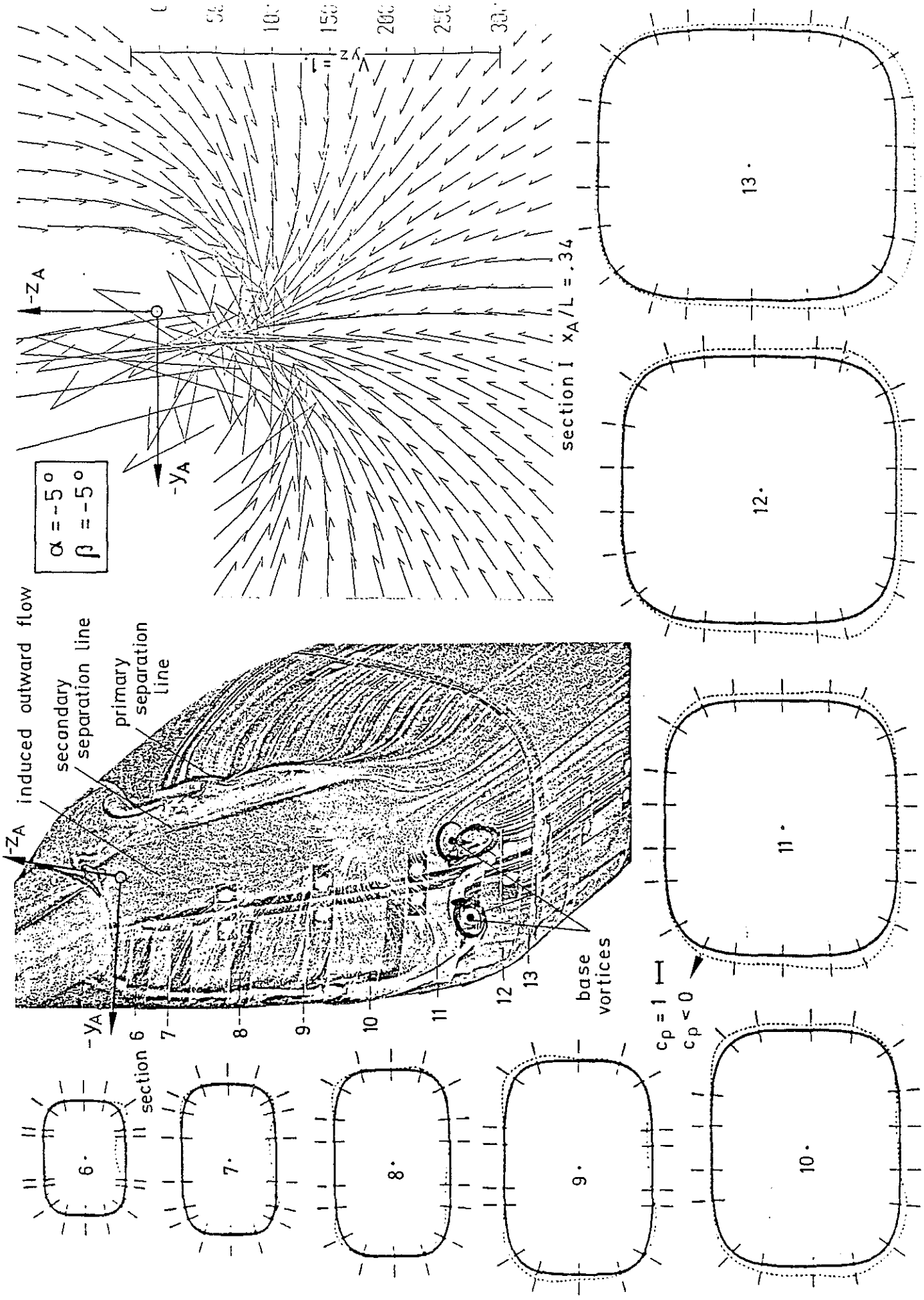

Fig. 10 Comparison of oil flow pictures, pressure distribution and wake survey results, ($\alpha = -5°$, $\beta = -5°$)

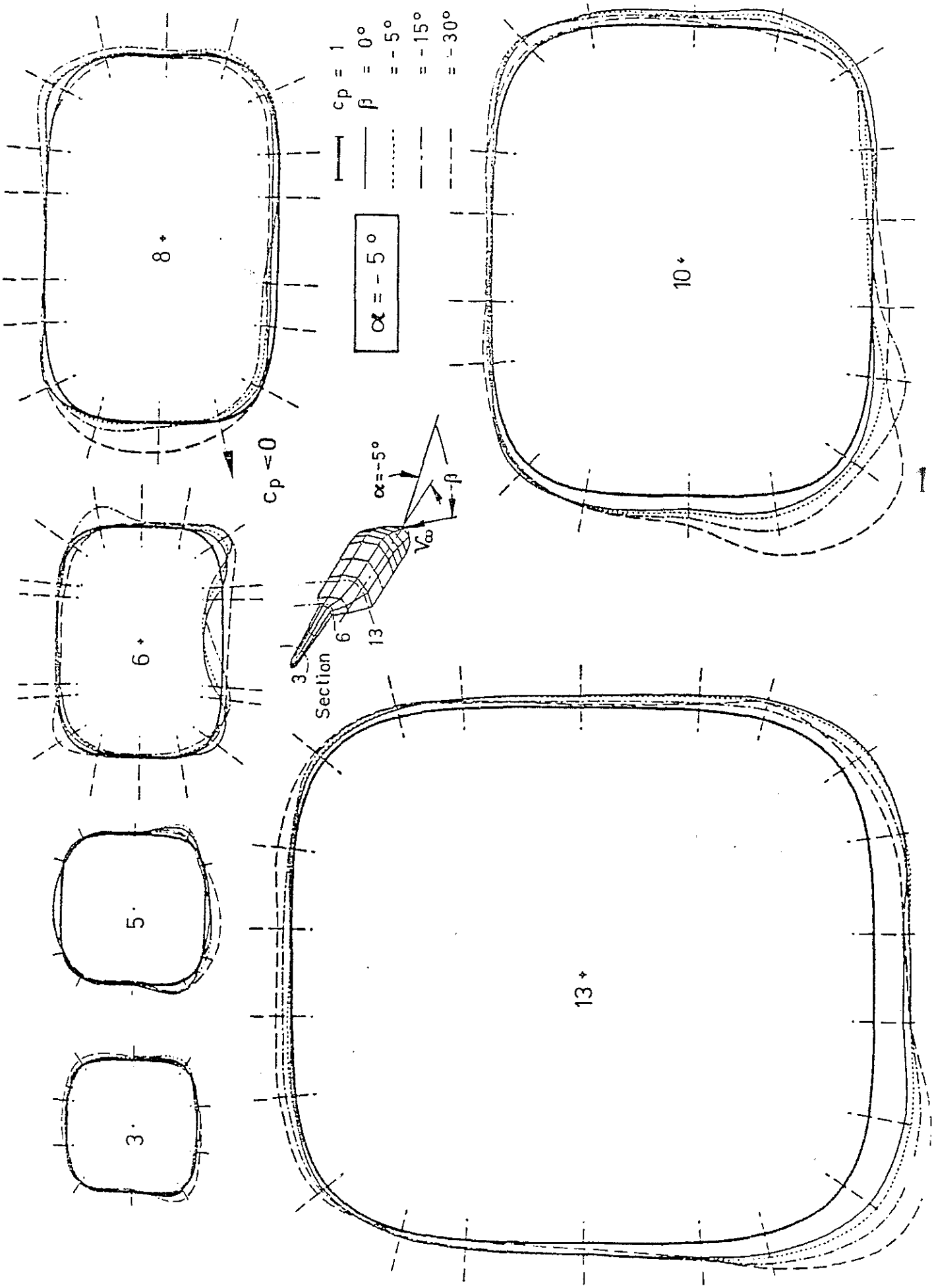

Fig. 11 Pressure distribution on cross sections of rear part, (influence of yaw angle)

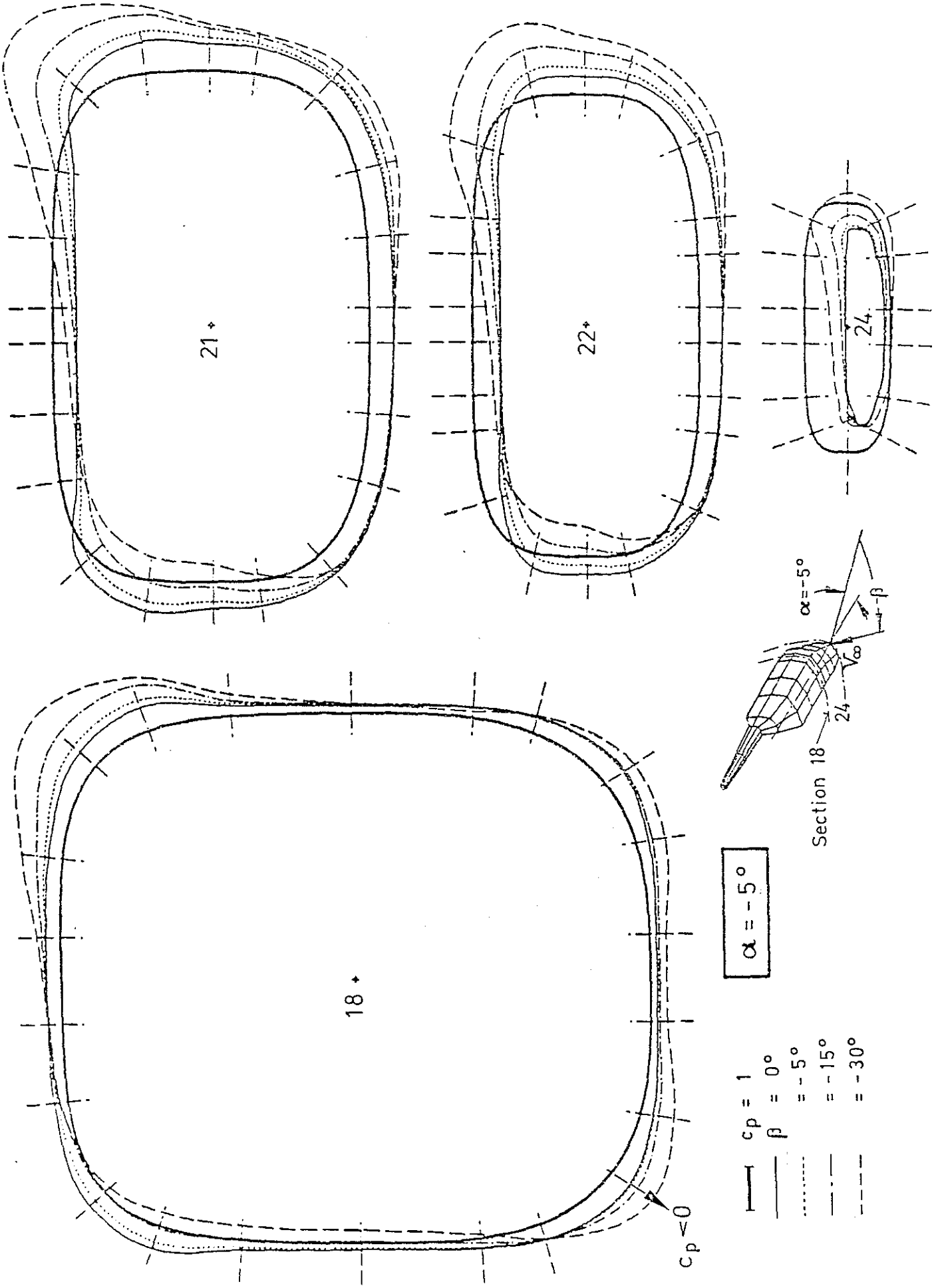

Fig. 12 Pressure distribution on cross-sections of front part, (influence of yaw angle)

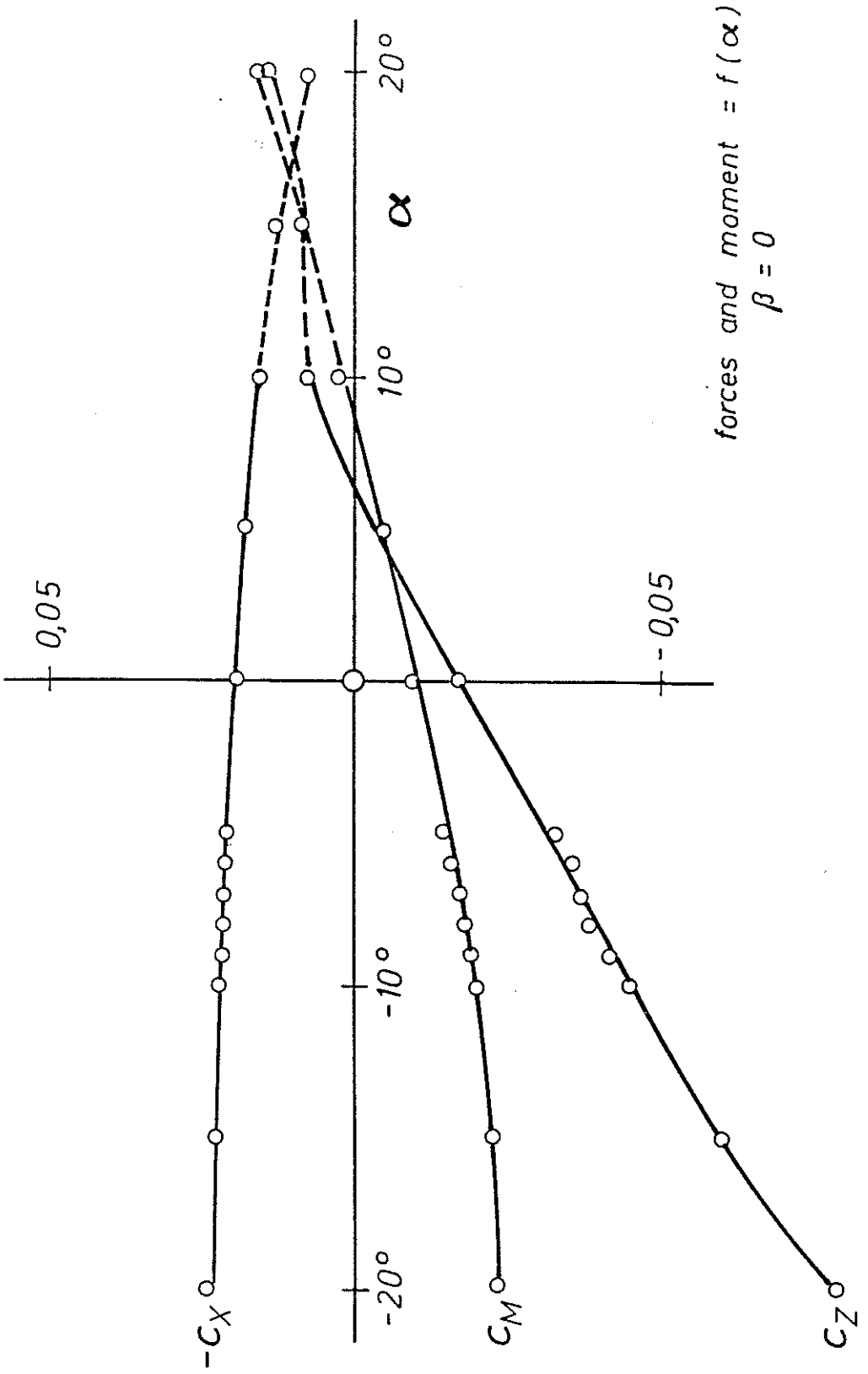

Fig. 13 Variation of aerodynamic coefficients C_X, C_Z and C_M with α ($\beta = 0^\circ$)